AIChE

Investigation of Nonuniformity in a Liquid–Solid Fluidized Bed with Identical Parallel Channels

Long Fan, John R. Grace, and Norman Epstein
Dept. of Chemical and Biological Engineering, University of British Columbia, Vancouver, BC, Canada V6T1Z3

DOI 10.1002/aic.11997
Published online September 14, 2009 in Wiley InterScience (www.interscience.wiley.com)

Previous work has demonstrated that multiphase flow through identical parallel channels and multiple cyclones can give rise to significant nonuniformity among the flow paths. This article presents results from a study where the distribution of voidage and flux through parallel channels in liquid–solid fluidized beds is investigated. Experiments and computational fluid dynamics simulations were performed with 1.2 mm glass beads fluidized by water where a cross baffle divided a 191 mm diameter column into four identical parallel channels. Voidages were measured by optical fiber probes. Simulations from a three-dimensional unsteady-state Eulerian–Eulerian model based on FLUENT software showed good agreement with the experimental results. Despite the symmetrical geometry of the system, the average voidage and particle velocities in one channel differed somewhat from those in the others. Increasing the superficial liquid velocity could increase voidage greatly and affect the degree of nonuniformity in the four channels. © 2009 American Institute of Chemical Engineers *AIChE J,* 56: 92–101, 2010
Keywords: nonuniform flow, liquid–solid, parallel channels, CFD, fluidization

Introduction

Multiphase flow is important in many engineering applications. Equipment for these operations takes many physical forms. When a single-phase fluid splits isothermally into identical parallel flow paths, which then recombine at a common destination, the requirement that the pressure drop should be identical through each of the paths results in a uniform distribution of the fluid among the channels. However, when two or more phases are present, it may be possible for there to be nonuniform flow distribution,[1] while still equalizing the pressure drops across the separate paths.

Evidence for this phenomenon has been available for many years (e.g., Smellie[2] and Koffman[3]), but it has received little attention until recently. Broodryk and Shingles[4] simulated industrial two- and three-cyclone geometries in cold model experimental units. Preferential flow patterns occurred in many cases, even leading to backflow and blockage of individual cyclones. The maldistribution improved but did not disappear at higher gas velocities and hence higher pressure drops. Schneider et al.[5] reported that maldistribution in pulverized fuel (PF) flow splitting devices was a major problem resulting in unequal oxygen and fuel connections in localized regions. Boyd et al.[6] encountered nonuniformity when operating an internally circulating gas-fluidized bed, where parallel vertical membrane panels were suspended within a draft box to create a series of parallel identical slots through which gas and particles were intended to circulate equally. In practice, some slots experienced much more gas and solids flow than others, causing the overall performance to suffer. Kuan and Yang[7] found nonuniformities in computational fluid dynamics (CFD) predictions of flow of conveyed gas–solid suspensions into a bifurcation. They predicted 5.7% and 9.2% more solids flow to one leg than the other for 66 and 77 μm particles, respectively.

Maldistribution can negatively affect industrial equipment, e.g., by causing decreased cyclone capture efficiency,[3,8]

Correspondence concerning this article should be addressed to L. Fan at longfanv@gmail.com

differential erosion, differential fouling and more frequent shutdowns. For example, early fluidized bed reactors for the production of ethylene oxide and hydrocarbon synthesis featured multiple open vertical heat transfer tubes of equal length and diameter through which the fluidized suspension was intended to pass uniformly. However, there was severe maldistribution, which plagued the reactor operation.[9] The system was inherently unstable and experienced serious problems. Similar phenomena have occurred in PF-fired boilers where a significant contributor to the inefficiency of PF-fired boilers can be unequal fuel distribution to the burners.[8] The pneumatic conveying pipeline that carries the PF from a mill to the furnace typically bifurcates two or three times to feed four or eight burners. If the amount of fuel being supplied to each burner differs, some will exhibit incomplete combustion and produce harmful emissions such as carbon monoxide gases, whereas others burn inefficiently with excess air. Consequently, the overall boiler efficiency is reduced.

Few solutions are available to solve these maldistribution problems. Holmes et al.[8] suggested five active techniques to control the split ratios, involving back pressure, flow diversion, and an active riffle box. By opening communication between adjacent fluidization channels, Grace et al.[10] solved the problem of maldistribution, which plagued earlier geometries of fluidized bed membrane reactors where parallel vertical chambers of equal dimensions were isolated from each other over their entire height. Cold modeling[11] also demonstrated that the nonuniformity could be alleviated by providing perforations or gaps between adjacent chambers.

The fluidized bed and conveyed suspension systems reviewed above all relate to gas–solid two-phase flows. Nonuniformity of gas–liquid two-phase flows in parallel paths has also been reported recently in the literature.[12] This article addresses, both experimentally and by CFD simulation, the question of whether nonuniformity can also occur for liquid–solid fluidized beds with identical parallel channels. This is important for two reasons: (a) to help elucidate the basic phenomena underlying maldistribution by significantly broadening the database of two-phase systems examined for nonuniformity, and (b) liquid–solid suspensions are important in their own right. If they are subject to maldistribution similar to that encountered for gas–solid and gas–liquid suspensions, this could represent a serious constraint in the design and operation of such systems.

Experimental Details

Various experimental methods have been used by different investigators to measure solids concentrations and particle velocities, e.g., particle image velocimetry, optical fiber probe, laser doppler anemometry, and phase doppler anemometry. Optical fiber methods are used more and more frequently. For example, Schweitzer et al.[13] investigated the local flow structure in a slurry bubble column and a fluidized bed with optical fiber probes to evaluate flow properties in gas–solid and gas–liquid–solid systems. Ellis et al.[14] studied the hydrodynamics of fluidized beds based on optical probe measurements. Liu et al.[15,16] developed a multifunctional optical fiber probe capable of determining local particle concentration, local particle velocity, and local solids flux simultaneously. They applied this technique to measurements in a high-density circulating fluidized-bed riser. Others in our laboratory (e.g., Freitas et al.,[17] Wang,[18] and Chen[19]) have successfully deployed optical fiber probes in a variety of systems. Therefore, optical fiber probes were used in the present work.

Equipment and materials

The experiments were performed in an acrylic liquid–solid fluidization column of 190.5 mm diameter and 900 mm height shown schematically in Figure 1. Water was pumped to the column from a reservoir containing several baffles to prevent bubbles from reaching the column. The distributor was composed of two perforated plates with 85 uniformly spaced orifices of diameter 4 mm. An acrylic vertical cross baffle (Figure 2) of height 250 mm and thickness 6.35 mm was installed inside to divide the column into four equal parallel channels, labeled left, right, front, and back as indicated. The distance between the top of the distributor plate to the bottom of the baffle was 150 mm. The static bed height was 450 mm, i.e., the static bed extended 50 mm above the cross baffle.

The liquid was water, and the solid particles were spherical glass beads of density 2500 kg/m^3 and diameter 1.2 mm with a narrow size distribution, as measured by a Malvern Mastersizer 2000.

Voidage measurements

Pressure ports on both sides of the column were connected to two pressure transducers (Omega model PX750),

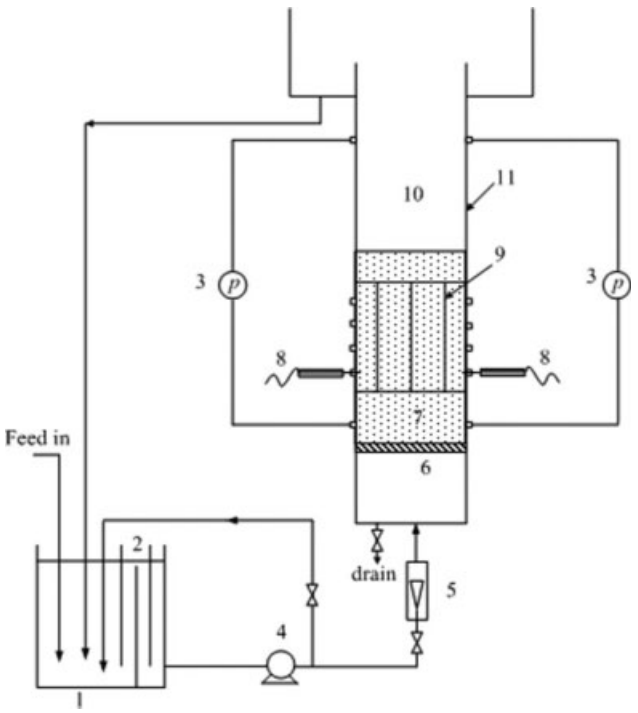

Figure 1. Experimental equipment. 1, reservoir; 2, baffle; 3, pressure transducer; 4, pump; 5, rotameter; 6, distributor; 7, fluidized bed; 8, optical fiber probe; 9, cross baffle; 10, freeboard; 11, fluidization column.

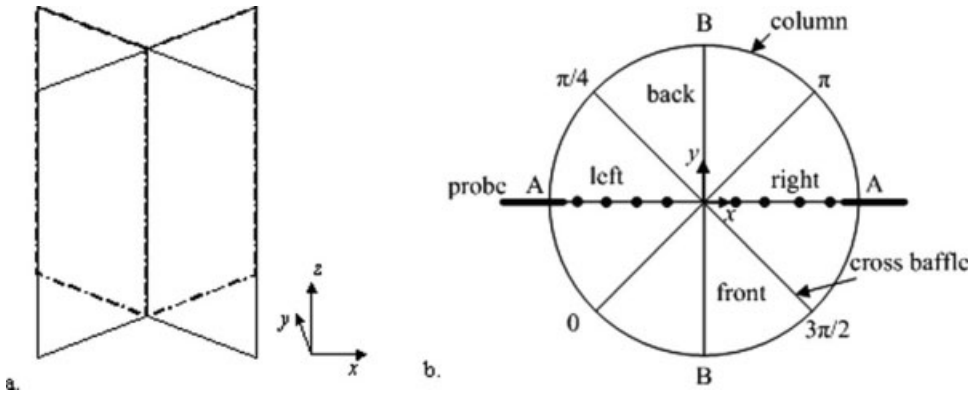

Figure 2. Structure of cross baffle. (a) structure, (b) top view.

respectively. Two ports were 75 mm above the bottom of the column, and two were 150 mm below the top of the column. Two rows of evenly spaced measurement ports were installed at 50 mm vertical intervals on opposite sides (left and right) of the column for insertion of optical fiber probes, as shown in Figures 1 and 2b, making it possible to measure and compare voidages in the left and right channels. The ports began 50 mm above the bottom of the baffle and ended 50 mm below the top of the baffle. For each measurement port, the probes were inserted and moved stepwise along the radial direction in 20 mm intervals, beginning 20 mm from the wall, as shown by the black dots in Figure 2b.

Voidages in the left and right channels were measured simultaneously using two identical instruments, PC-4 Powder Voidmeter, manufactured by the Institute of Process Engineering (Chinese Academy of Sciences, Beijing). This instrument consisted of an optical fiber probe, a light source, a photomultiplier, and an A/D converter for data acquisition. At the tip of the probe, light projecting fibers were interspersed with light-receiving fibers. The reflected light intensity, related to the particle concentration in front of the probe tip, was converted to an electrical signal. The electrical signal was saved on the computer automatically during measurements with both pressure and voidage data sampled at 100 Hz for periods of 150 s. The voidage at minimum fluidization, ε_0, was determined to be 0.40 with a graduated cylinder. The minimum fluidization velocity was 0.011 m/s.

According to He,[20] the voidage in a system of relatively large particles (e.g., diameter > 1.2 mm) is linearly proportional to the intensity of reflected light. A similar linear relationship was found for our water—1.2 mm glass beads system. Data were read in a column full of water and in a loose-packed bed with the voidages at these two conditions assumed to be 1.0 and ε_0. Using the linear function between the voidage and intensity of reflected light, intermediate voidages could be estimated.

CFD Model

Simulation methods

According to Cornelissen et al.,[21] unless an appropriate turbulence model with the correct empirical constants and closures is chosen, turbulent model predictions for fluidized beds may be less consistent with experimental data than a laminar model. For our system, all Reynolds numbers ($Re = d_p\, u\rho/\mu$) were <100. Therefore, a laminar flow model was adopted.

A three-dimensional unsteady state Eulerian–Eulerian model was used to simulate the liquid–solid two-phase flow in a fluidized bed. The kinetic theory of granular flow[22] was used for the solid phase. The drag force between solid and liquid was obtained from the equation of Wen and Yu.[23] The equation of Lun et al.[24] provided the granular bulk viscosity. The expression of Schaeffer[25] was used for frictional viscosity, with an angle of internal friction of 30°.[26]

The unsteady-state, three-dimensional continuity equation, and momentum equations

$$\frac{\partial}{\partial t}\left(\alpha_q \rho_q\right) + \nabla\left(\alpha_q \rho_q \vec{u_q}\right) = 0 \tag{1}$$

$$\frac{\partial}{\partial t}\left(\alpha_l \rho_l \vec{u_l}\right) + \nabla \cdot \left(\alpha_l \rho_l \vec{u_l}^2\right) = -\alpha_l \nabla p + \nabla \cdot \overline{\overline{\tau_l}} + \alpha_l \rho_l \vec{g} + K_{sl}\left(\vec{u_s} - \vec{u_l}\right) \tag{2}$$

$$\frac{\partial}{\partial t}\left(\alpha_s \rho_s \vec{u_s}\right) + \nabla \cdot \left(\alpha_s \rho_s \vec{u_s}^2\right) = -\alpha_s \nabla p + \nabla p_s + \nabla \cdot \overline{\overline{\tau_s}} + \alpha_s \rho_s \vec{g} + K_{ls}\left(\vec{u_l} - \vec{u_s}\right) \tag{3}$$

where

$$\overline{\overline{\tau_q}} = \alpha_q \mu_q \left(\nabla \cdot \vec{u_q} + \nabla \cdot \vec{u_q}^T\right) + \alpha_q \left(v_q - \frac{2}{3}\mu_q\right) \nabla \cdot \vec{u_q} \overline{\overline{I}} \tag{4}$$

were solved by the commercial CFD code FLUENT 6.3.26 based on the laminar flow option in double precision mode. Gambit[26] was used for grid generation. The sum of volume fraction of solid phase and liquid phase is unity, i.e.,

$$\alpha_s + \alpha_l = 1 \tag{5}$$

No slip boundary conditions were imposed at all solid surfaces. The liquid was assumed to be distributed perfectly uniformly across the distributor cross section as the water entry boundary condition. The thickness of each partition was taken as 6.35 mm, as in the experimental tests.

Solution methods

The equations were discretized using the first-order upwind scheme and solved by the SIMPLE algorithm.[27] The nonlinearity in the phase momentum equations was dealt with by under relaxation. When the residuals of each of the equations met the prescribed tolerance of a change of $<0.1\%$ from the previous iteration, a converged solution was considered to have been obtained.

Experimental Results and CFD Predictions

CFD simulations were performed for a geometry identical to the experimental one. A bed of static height 450 mm was impulsively fluidized with a uniform liquid superficial velocity of 0.026 m/s beginning at time zero. Based on Cornelissen et al.,[21] a time step of 0.001 s was used in the simulations.

For simplicity, several planes were considered in analyzing the data. The plane at $y = 0$ mm is the central plane through the column, as illustrated in Figure 2b. Lines with $z = 275$ mm in the plane $y = 0$ mm and with $z = 275$ mm in the plane $x = 0$ mm are labeled A-A and B-B, respectively. Except where specified otherwise, average voidages or solid velocities in the left and right channels below denote averages on line A-A, whereas averages in the front and back channels refer to average values along line B-B.

Choice of grids

The choice of CFD grid can influence the simulation significantly. Three grids were tested in our simulations with 30,125, 65,038, and 89,433 intersection points. It was found that the results for grids of 65,038 points were very similar to those for 89,433 grid points. Hence, 65,038 grid points were chosen for the simulations presented here.

Figure 3 shows the evolution of average voidage with time in the left and right channels for a superficial water velocity of 0.026 m/s. After 120 s, the voidages in the two channels approached similar steady state values, although

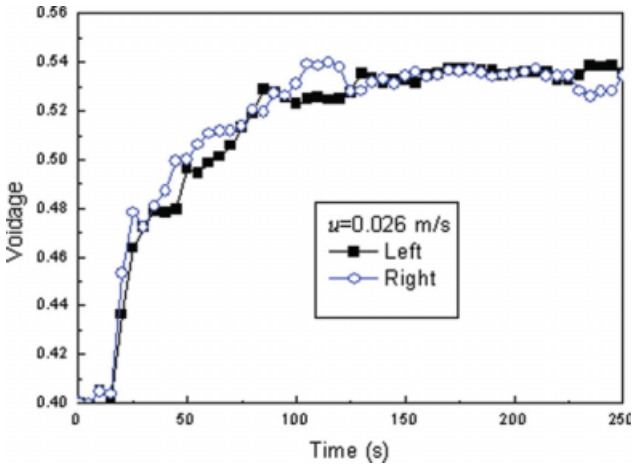

Figure 3. Evolution of simulated voidage with time in left and right regions.

[Color figure can be viewed in the online issue, which is available at www.interscience.wiley.com.]

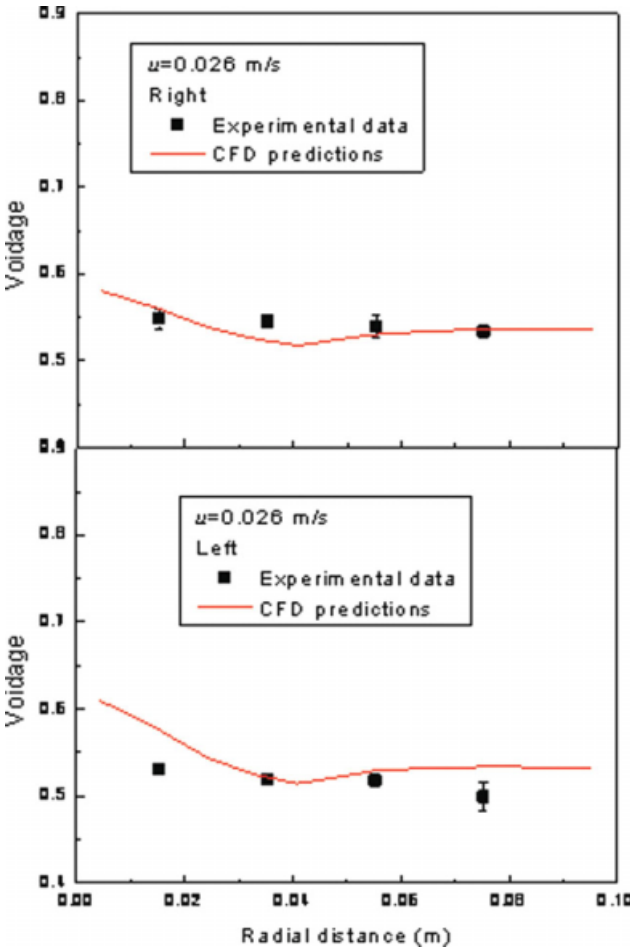

Figure 4. Comparison of voidage between simulations and experiments in the left and right channels.

[Color figure can be viewed in the online issue, which is available at www.interscience.wiley.com.]

with some fluctuations. The voidage changed little from 150 to 250 s. Therefore, the simulation was considered to have reached steady state by 150 s. All time-averaged results below were averaged over a time period extending from 150 to 250 s.

Experimental results and verification of simulations

Experiments and simulations carried out with no baffle in place in the same column under the same operating conditions confirmed that there was no statistical difference between the same four quadrants as were examined when the cross baffle was in place.

Figure 4 compares the experimental and simulated time-averaged voidages at $z = 0.25$ m in the center of the left and right regions. Simulated pressure drops for the left and right channels were virtually the same, as expected, and within about 3% of the experimental results.

Voidage distributions

Figure 5a shows the simulated volume fraction of solid phase in the vertical $y = 0$ mm plane at 150 s, indicating an uneven instantaneous distribution of solids in the two

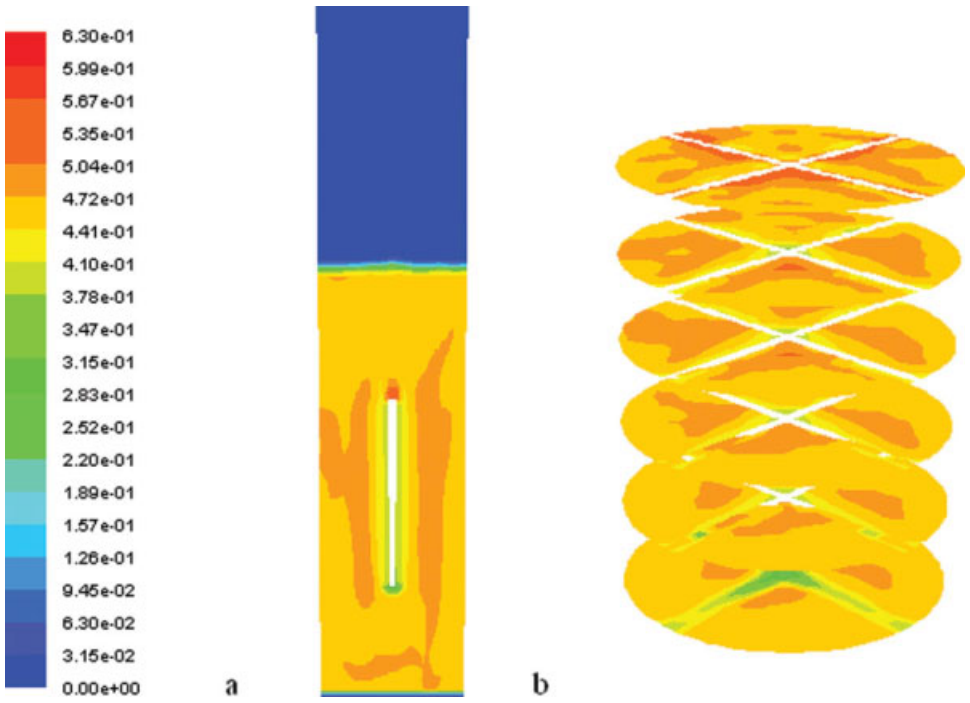

Figure 5. Distribution of simulated volume fraction of solid phase, (a) in the vertical plane of $y = 0$ mm, (b) in different horizontal planes along z axis.

[Color figure can be viewed in the online issue, which is available at www.interscience.wiley.com.]

opposite channels. Figure 5b plots the distribution of solid phase in different horizontal planes along the z-axis, i.e., at $z = 150$, 200, 250, 300, 350, and 400 mm, with the baffle beginning at $z = 150$ mm and ending at $z = 400$ mm. Although the incoming water is assumed to be distributed perfectly uniformly, it is seen that the solid phase is distributed unevenly in the four channels at this instant.

The simulated average voidages on line B-B in the front and back channels are plotted in Figure 6. Despite the similarity of the voidages in the left and right channels, the voidages in the front and back channels were predicted to differ slightly from each other. The time-averaged voidage at steady state in the back channel was 0.537, close to those of the left and right channels, whereas that in the front region was 0.530. Although the four channels had the same shape and volume, the distributions of solid phase were nonuniform. Compared with the results of Kuan and Yang[7] for a gas–solid system, the difference of 1.3% is relatively small.

To test for the presence of the nonuniformity, a student t-test was performed for the time-averaged voidages on lines A-A and B-B. The data at three radial locations were chosen for the test, i.e., $r = 0.0149$, 0.0547, and 0.0871 m. In the left and right regions, the time-averaged voidages at $r = 0.0547$ m were judged to be the same, as were those at $r = 0.0871$ m, whereas the voidages at $r = 0.0149$ m differed, all at a 99% confidence level. However, for the front and back regions, the voidages at both $r = 0.0149$ m and $r = 0.0871$ m showed differences at the 99% confidence level.

Figures 7 and 8 show the radial variation of time-averaged voidage at $z = 350$ mm. There is again seen to be good agreement between the experimental and CFD predicted voidages. For $r \leq 0.04$ m, the voidages decreased gradually with increasing r in the left, right, and back channels, whereas for $r > 0.04$ m, the voidage was nearly constant. This may occur because smaller radial distances correspond to closer approach to the center of the column and hence to the cross baffle, the double wall effect of that causes the voidage to increase. However, the voidage in the front channel did not vary as much near the center as in the other channels, as shown in Figure 8.

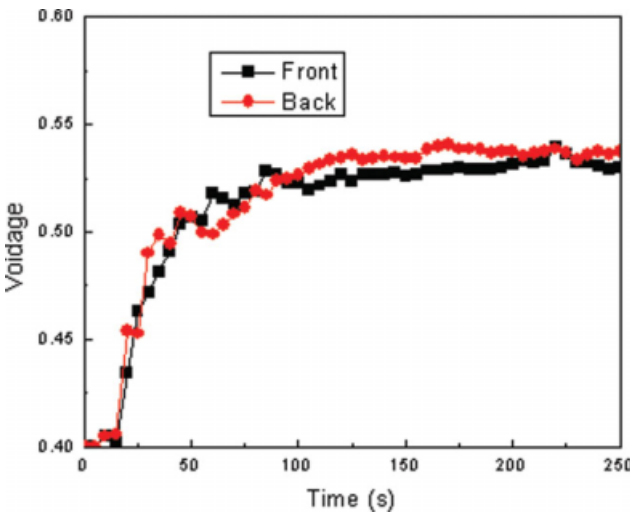

Figure 6. Evolution of predicted voidages in the front and back channels.

[Color figure can be viewed in the online issue, which is available at www.interscience.wiley.com.]

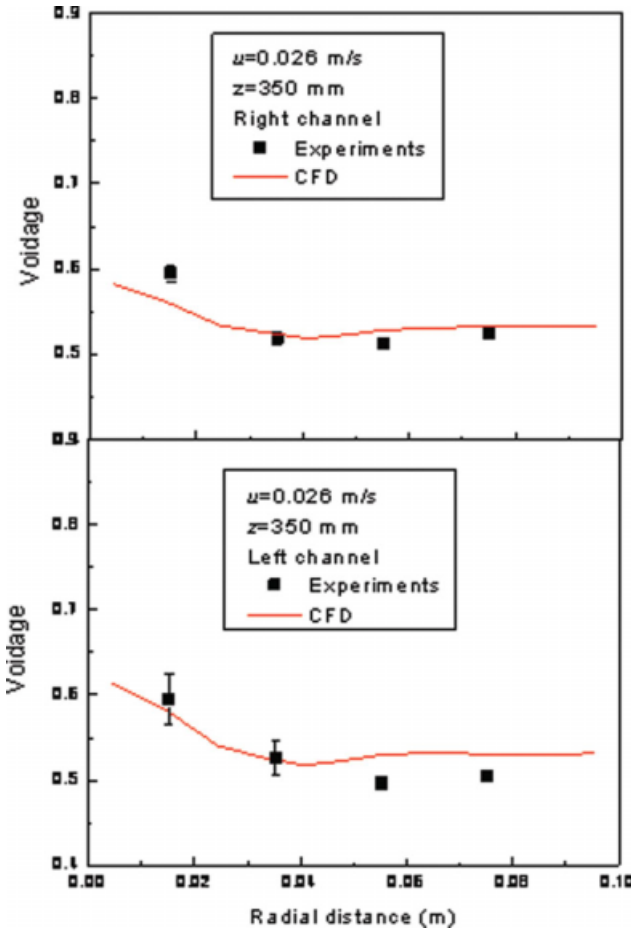

Figure 7. Relationship between the voidage and the radial distance in the left and right channels.

[Color figure can be viewed in the online issue, which is available at www.interscience.wiley.com.]

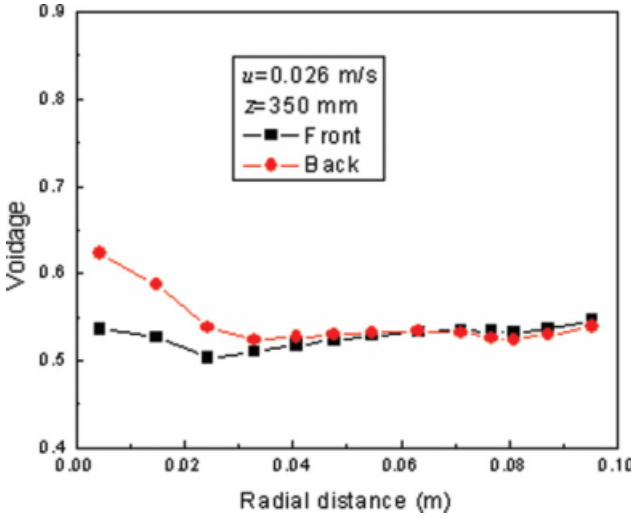

Figure 8. Relationship between the simulated voidage and the radial distance in front and back channels.

[Color figure can be viewed in the online issue, which is available at www.interscience.wiley.com.]

To visualize the difference among the four channels more clearly, the predicted voidage is plotted vs. angle in Figure 9 at $r = 60$ and 90 mm, with the left channel extending from 0 to $\pi/2$ radians, and the back, right, and front channels covering $\pi/2$ to π radians, π to $3\pi/2$, and $3\pi/2$ to 2π radians, respectively. The plane at $z = 275$ mm, midway up the baffle, is chosen for analysis. The voidage near the baffle was larger in all four channels, presumably because particles were unable to pack as tightly in the vicinity of a flat surface. The four channels give similar profiles at both radial locations, but they are not identical, reflecting fluctuations with angle and radial distance.

Solids velocity and flux distribution

Time variations of averaged solid velocity and solid flux were also predicted by the CFD model. Figure 10 plots the instantaneous spatially averaged solid flux, $(1\text{-}\varepsilon)u_z$, along line A-A as function of time. The velocity and flux of the solid phase are predicted to fluctuate with time more than the voidage, even after statistical steady state has been achieved, as illustrated by comparing Figure 10 for solid flux with Figure 6 for voidage.

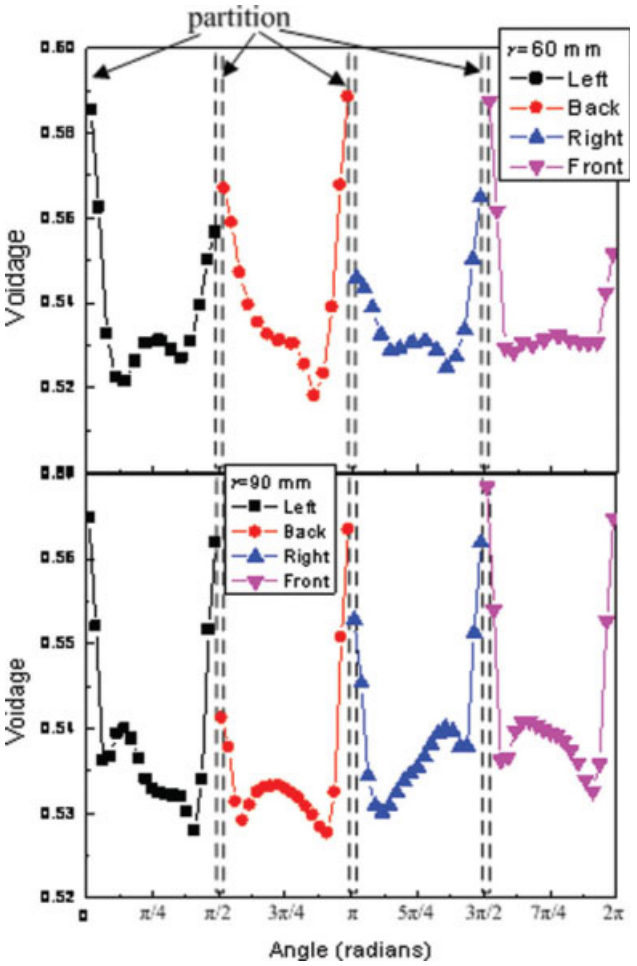

Figure 9. Profile of CFD-predicted time-averaged voidage vs. angle at r = 60 and 90 mm.

[Color figure can be viewed in the online issue, which is available at www.interscience.wiley.com.]

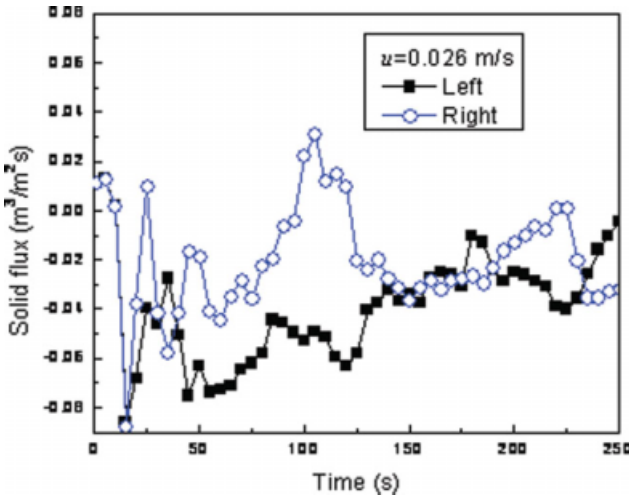

Figure 10. Variation of simulated instantaneous spatially averaged solid flux with time in left and right channels.

[Color figure can be viewed in the online issue, which is available at www.interscience.wiley.com.]

The relationship between time-averaged solid velocity and angle for a superficial velocity of 0.026 m/s is plotted in Figure 11 for the same two radii as in Figure 9. Less symmetry was observed in the relationships between solid velocity (or flux) and angle than for voidage. The predicted particle velocity fluctuated with angle and radial position. For $r = 60$ mm, the particle velocities in the left, back, and right regions were similar. Particles rose near the baffle and descended in the middle of these channels, reaching a maximum negative velocity approximately midway between neighboring baffles. The positive velocity near the outer edges of each chamber are likely related to the higher voidage there as portrayed in Figure 9, allowing more liquid to ascend in these regions. The front channel differed from other channels, with particles in this channel mostly ascending. At $r = 90$ mm, the flows in the left and back channels were similar to those at $r = 60$ mm, with particles descending in the middle and ascending near the baffles. As for the right and front channels, solid velocities were almost all positive, especially in the front channel, indicating some nonuniformity in the liquid–solid fluidized bed with parallel channels, consistent with visual observations.

Influence of superficial velocity

The influence of superficial velocity was also investigated both experimentally and by simulations. Figure 12 compares time-averaged voidage in the horizontal plane with $z = 250$ mm and $y = 0$ mm in the left channel, where the lines show CFD predictions and the points are experimental data. With increasing superficial velocity, both the experimental and simulated voidages increased as expected. There were small differences between the simulated voidages and the experimented data, with the discrepancies decreasing with increasing superficial velocity. Similar results, not shown here, were obtained for the right channel.

Figure 13 shows that the simulated time-averaged voidages in the front and back channels also increased with

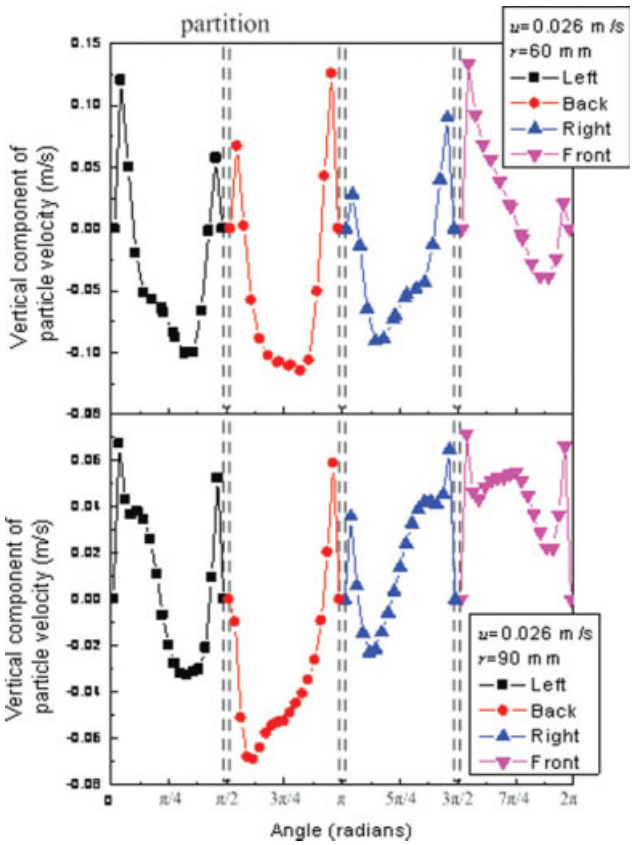

Figure 11. Profile of CFD-predicted time-averaged solid velocity and angle with r = 60 and 90 mm.

[Color figure can be viewed in the online issue, which is available at www.interscience.wiley.com.]

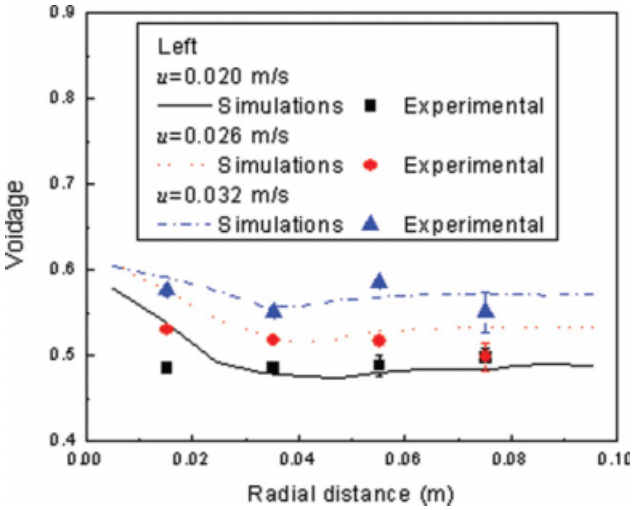

Figure 12. Influence of superficial velocity on experimental and predicted voidages for left channel.

[Color figure can be viewed in the online issue, which is available at www.interscience.wiley.com.]

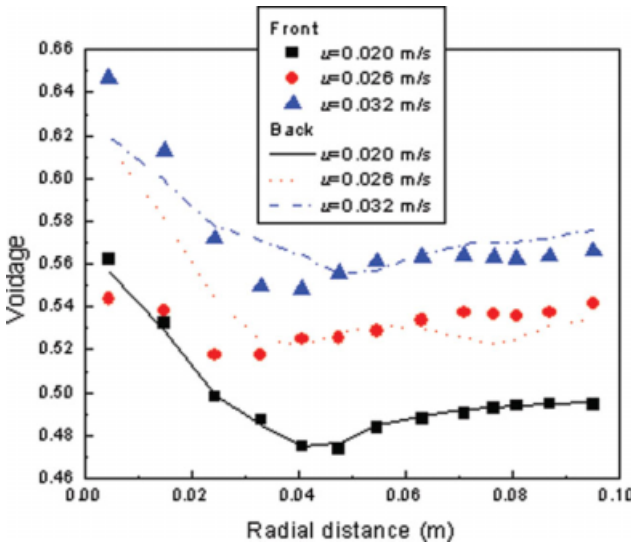

Figure 13. Predicted influence of superficial velocity on voidage in front and back channels.

[Color figure can be viewed in the online issue, which is available at www.interscience.wiley.com.]

increasing superficial liquid velocity. For $u = 0.020$ m/s, the voidages in the front and back regions were predicted similar, but higher superficial velocities of 0.026 and 0.032 m/s led to appreciable differences between the voidages in the front and back channels near the center. At $u = 0.026$ m/s, the voidage in the front channel was smaller than in the back channel by up to 12%, whereas at $u = 0.032$ m/s, the voidage in the front channel was larger than in the back channel by up to 5%.

The effects of superficial velocity can be seen clearly in the relationship between voidage and angle. Figure 14 shows the simulated time-averaged voidage vs. angle in four channels at three different superficial velocities and at $r = 60$ mm. The voidages in all four channels increased significantly when the superficial velocity was raised from 0.020 to 0.032 m/s. Symmetry occurred between the voidages in two opposite regions at 0.020 m/s, viz. the back region ($\pi/2$ to π radians) and the front region ($3\pi/2$ to 2π radians), but the symmetry decreased with increasing superficial liquid velocity.

The effect of superficial velocity on time-averaged solid velocity is plotted in Figure 15 for $r = 60$ mm. In the middle of the left channel, solid velocity increased with superficial velocity, whereas in the other channels, it did not have a consistent trend with superficial velocity.

Discussion

All four channels had the same shape and volume, and the distributor at the inlet was uniform. What triggered the small nonuniformity in this fluidized bed? Elnashaie and Grace[28] note that multiple steady-state solutions are possible for many situations, where there is nonlinearity. Some of these solutions are unstable and unlikely to be found in practice.

For liquid–solid fluidized beds, the pressure drop through each channel is primarily a function of the solids hold up (gravity) but is also influenced to some extent by wall

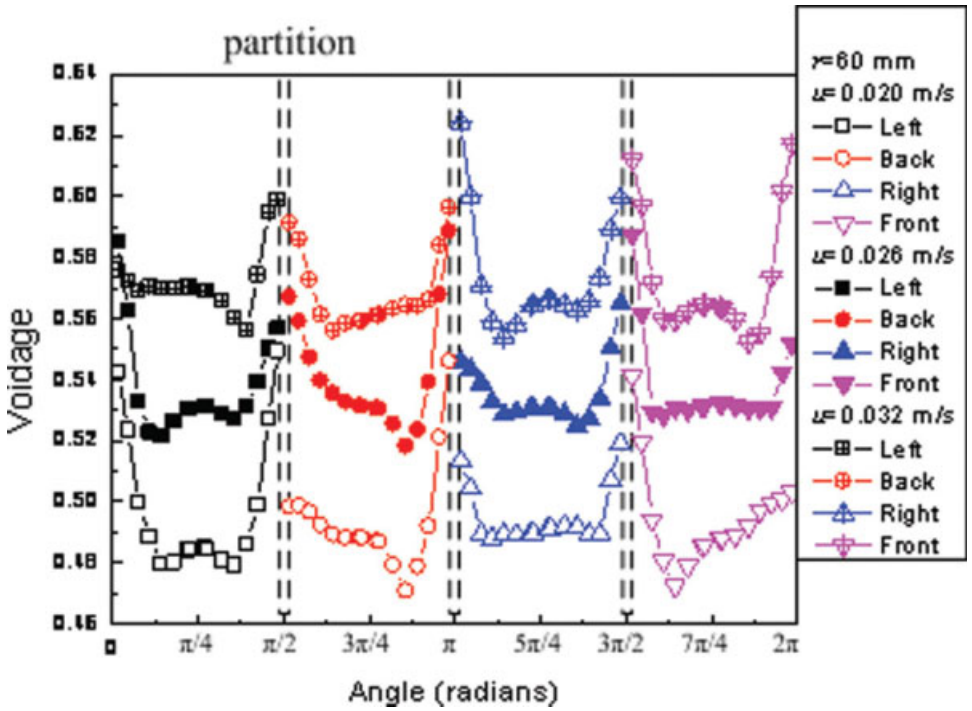

Figure 14. Influence of superficial velocity on the relationship between CFD-predicted time-averaged voidage and angle at $r = 60$ mm.

[Color figure can be viewed in the online issue, which is available at www.interscience.wiley.com.]

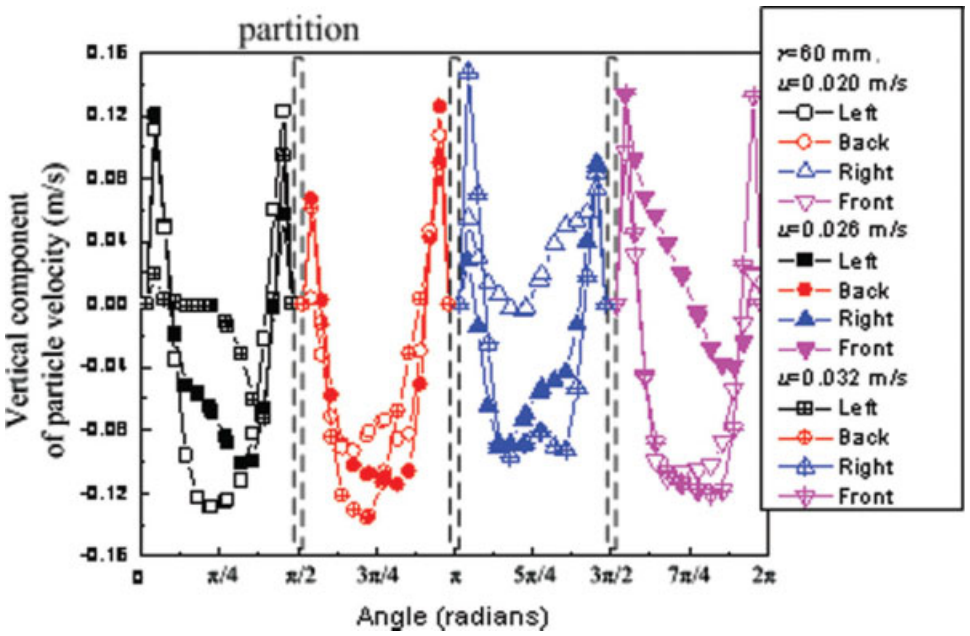

Figure 15. Influence of superficial velocity on the relationship between CFD-predicted time-averaged particle velocity and angle for $r = 60$ mm.

[Color figure can be viewed in the online issue, which is available at www.interscience.wiley.com.]

friction. The frictional pressure drop is related to the shear stress for steady state by

$$\Delta p_F = \frac{4L}{D}\tau_0 \tag{6}$$

where τ_0 is the shear stress at the wall. Rose and Duckworth[29] wrote

$$\tau_0 = \lambda \rho_l u^2/8 \tag{7}$$

with

$$\lambda = \frac{\Delta p_F}{(\rho_l u^2/2)L/D} - 2\left(\frac{gD}{u^2}\right)\sin\theta\left[1 + M^*\left(\frac{u}{u_s}\right)\left(1 - \frac{\rho_l}{\rho_s}\right)\right] \tag{8}$$

For our system, $\sin\theta = \sin(\pi/2) = 1$. It is seen that the friction loss is a nonlinear function of liquid velocity.

The combination of pressure drop through the bed due to particle drag and wall friction loss makes the total pressure drop a complicated nonlinear function of velocity and voidage. Even though the pressure drops through the bed in different channels are the same, the voidages and velocities in different channels may differ. However, the results of this study indicate that the degree of difference seems to be considerably smaller for the liquid–solid system than for gas–solid systems, at least for the range of conditions investigated. The reason for this difference is likely associated with wall friction being a significantly smaller proportion of the gravitational (weight minus buoyancy) pressure drop for liquid–solid systems than for conveyed gas–solid systems, meaning that it is more difficult for frictional effects to make up for differences in solids holdups in adjacent flow channels.

Conclusions

This article investigates the nonuniformity in a liquid–solid fluidized bed with parallel channels both experimentally and by three-dimensional unsteady-state Eulerian–Eulerian CFD simulation based on FLUENT software.

The CFD voidage simulations for the water fluidization of glass beads agreed well with the experimental voidages measured by optical fiber probes. Although the four parallel channels were identical and the distributor was uniform, the flows in the four channels differed somewhat, not only in voidage but also in solid velocity and solid flux, with one of the four channels tending to have more upward solids flow than the others. The nonuniformity in this particulately fluidized bed with parallel channels tended to increase as the superficial velocity increased.

Overall, our results suggest that liquid–solid fluidized beds, like gas–solid fluidized beds and gas–liquid suspensions, can exhibit nonuniformity in flow through multiple identical parallel channels. However, the distribution is likely to be significantly less nonuniform in the liquid–solid case because of the reduced importance of wall friction relative to the net gravity term in the pressure balance, with the result that serious maldistribution is unlikely to be a serious problem for liquid–solid fluidized beds under normal operating conditions.

Acknowledgments

Financial assistance from the Natural Sciences and Engineering Research Council of Canada (NSERC), the Canada Research Chairs program, and Syncrude Canada Limited are gratefully acknowledged.

Notation

d_p = diameter of particles, m
D = column diameter, m
g = acceleration of gravity, m/s^2
$\bar{\bar{I}}$ = stress tensor
K = interphase exchange coefficient
L = height of bed, m
M^* = mass flow ratio of solid to liquid
p = pressure, Pa
Δp_F = friction loss, Pa
u = superficial velocity, m/s
r = radial distance from center, m
t = time, s
x, y, z = Cartesian coordinates, with z vertical and measured from distributor, as shown in Figure 2, m
α = volume fraction
ε = voidage
θ = inclination of pipe to the horizontal, radians
λ = friction factor
μ = liquid viscosity, Pa s
υ = bulk viscosity, Pa s
ρ = density, kg/m^3
τ = shear stress, Pa

Subscripts

l = liquid phase
q = either liquid or solid phase
s = solid phase

Literature Cited

1. Grace JR, Cui HP, Elnashaie SSEH. Non-uniform distribution of two-phase flows through parallel identical paths. *Can J Chem Eng*. 2007;85:662–668.
2. Smellie J. Notes on dust suppression and collection. *Iron Coal Trades Rev*. 1942;144:227.
3. Koffman JL. The cleaning of engine air (Part 2). *Gas Oil Power*. 1953;89–94.
4. Broodryk NJ, Shingles T. Aspects of cyclone operation in industrial chemical reactors. Presented at the *Preprints for Fluidization VIII Conference*, Tours, France, May 1995:1083.
5. Schneider H, Frank T, Pachler K, Bernert K. *A numerical study of the gas-particle flow in pipework and flow splitting devices of coal-fired power plant*. In: Sommerfeld M, editor. *Proc 10th Workshop on Two-Phase Flow Predictions*. Merseburg, Germany: Martin-Luther-University, 2002;227–236.
6. Boyd DT, Grace JR, Lim CJ, Adris AM. Hydrogen from an internally circulating fluidized bed membrane reactor. *Int J Chem Reactor Eng*. 2005;3:A58.
7. Kuan BT, Yang W. Mal-distribution of coals in lignite-fired power station mill ducts: CFD simulations and experimental validation. Presented at the *International Conference on Coal Science and Technology*, Okinawa, Japan, October 2005.
8. Holmes T, Bradley MSA, Selves RJ, Bridle I, Reed AR. Techniques for control of splitting ratios of particulate materials at bifurcations in pneumatic conveying pipelines. *Proc Inst Mech Eng A*. 2000;214:657–667.
9. Bolthrunis CO, Silverman RW, Ferrari DC. *Rocky road to commercialization: breakthroughs and challenges in the commercialization of fluidized bed reactors*. In: Arena U, Chirone R, Miccio M, Salatino P, editors. *Fluidization XI*. Brooklyn, NY: Engineering Conferences International, 2004:547–554.
10. Grace JR, Lim CJ, Adris AM, Cui H, Boyd DA. Communicating compartment —alized fluidized bed reactor, US Patent 60/866247, 2006.
11. Boyd DT, Grace JR, Lim CJ, Adris AM. Cold modeling of an internally circulating fluidized bed membrane reactor. *Int J Chem Reactor Eng*. 2007;5:A26.
12. Zhang LF, Du W, Bi HT, Wilkinson DP, Stumper J, Wang HJ. Gas-liquid two-phase flow distributions in parallels for fuel cells. *J Power Sources*. 2009;189:1023–1031.
13. Schweitzer JM, Bayle J, Gauthier T. Local gas hold-up measurements in fluidized bed and slurry bubble column. *Chem Eng Sci*. 2001;56:1103–1110.
14. Ellis N, Briens LA, Grace JR, Lim CJ. Characterization of dynamic behavior in gas–solid turbulent fluidized bed using chaos and wavelet analyses. *Chem Eng J*. 2003;96:105–116.
15. Liu JZ, Grace JR, Bi XT. Novel multifunctional optical-fiber probe. I. Development and validation. *AIChE J*. 2003;49:1405–1420.
16. Liu JZ, Grace JR, Bi XT. Novel multifunctional optical-fiber probe. II. High-density CFB measurements. *AIChE J*. 2003;49:1421–1432.
17. Freitas LAP, Mitsutani K, Lim CJ, Grace JR, Wei WS. Voidage profiles in a slot-rectangular spouted bed. *Can J Chem Eng*. 2004;82:74–82.
18. Wang ZG. Experimental Studies and CFD Simulations of Conical Spouted Bed Hydrodynamics, PhD Thesis. Vancouver, Canada: University of British Columbia, 2006.
19. Chen ZW. Hydrodynamics, Stability and Scale-Up of Slot-Rectangular Spouted Beds, PhD Thesis. Vancouver, Canada: University of British Columbia, 2008.
20. He Y. Hydrodynamic and Scale-Up Studies of Spouted Beds, PhD Thesis. Vancouver, Canada: University of British Columbia, 1995.
21. Cornelissen JT, Taghipour F, Escudié R, Ellis N, Grace JR. CFD modelling of a liquid–solid fluidized bed. *Chem Eng Sci*. 2007;62:6334–6348.
22. Gidaspow D. *Multiphase Flow and Fluidisation*, London: Academic Press, 1994.
23. Wen CY, Yu YH. Mechanics of fluidization. *Chem Eng Prog Symp Ser*. 1966;62:100–111.
24. Lun CKK, Savage SB, Jeffrey DJ, Chepurniy N. Kinetic theories for granular flow: inelastic particle in Couette flow and slightly inelastic particles in a general flow field. *J Fluid Mech*. 1984;140:223–256.
25. Schaeffer DG. Instability in the evolution equations describing incompressible granular flow. *J Differ Equat*. 1987;66:19–50.
26. FLUENT Inc. *FLUENT 6.1 User's Guide*. Lebanon, NH: FLUENT Inc, 2003.
27. Patankar SV. *Numerical Heat Transfer and Fluid Flow*. New York: McGraw Hill, 1980.
28. Elnashaie SSEH, Grace JR. Complexity, bifurcation and chaos in natural and man-made lumped and distributed systems. *Chem Eng Sci*. 2007;62:3295–3325.
29. Rose HE, Duckworth RA. *The fluid transport of powdered materials in pipelines*. I. Chem. E. Symposium Series, No. 27, London: The Institution of Chemical Engineers, 1968:53–64.

Manuscript received Mar. 19, 2009, and revision received May 18, 2009.